Computational generation of the Purkinje network driven by clinical measurements: The case of pathological propagations

Simone Palamara[1,*,†], Christian Vergara[2], Domenico Catanzariti[3], Elena Faggiano[1,4], Cesarino Pangrazzi[3], Maurizio Centonze[5], Fabio Nobile[6], Massimiliano Maines[3] and Alfio Quarteroni[7]

[1]*Modellistica e Calcolo Scientifico (MOX), Dipartimento di Matematica, Politecnico di Milano, Milan, Italy*
[2]*Dipartimento di Ingegneria Gestionale, dell'Informazione e della Produzione, Università di Bergamo, Dalmine, BG, Italy*

[3]*Divisione di Cardiologia, Ospedale S. Maria del Carmine, Rovereto, TN, Italy*
[4]*Laboratory of Biological Structure Mechanics (LaBS), Dipartimento di Chimica, Materiali e Ingegneria Chimica, Politecnico di Milano, Milan, Italy*

[5]*U.O. di Radiologia di Borgo-Pergine, Ospedale di Borgo Valsugana, Borgo Valsugana, TN, Italy*
[6]*SB SMA-GE, École Polytechnique Fédérale de Lausanne, MA B2 444(Bâtiment MA), Lausanne, Switzerland*
[7]*SB SMA MATHICSE-CMCS, École Polytechnique Fédérale de Lausanne, Lausanne, Switzerland*

1. INTRODUCTION

The development of biophysical patient-specific models of the human heart is crucial to gain better insight on the mechanisms regulating its activity and to provide the clinicians with a powerful instrument for diagnosis and therapeutic design. In this context, a key aspect is the study of the electrical activation that triggers the heart contraction. This activity is regulated by the cardiac conduction system (CCS), responsible for the fast and coordinated distribution of the electrical impulse in the heart [1]. In particular, the ventricular activation is regulated by the peripheral part of the CCS, the Purkinje fibers (PF), located in the inner ventricular walls of the heart, just beneath

*Correspondence to: Simone Palamara, Modellistica e Calcolo Scientifico (MOX), Dipartimento di Matematica, Politecnico di Milano, Piazza Leonardo da Vinci 32, I-20133, Milan, Italy.
†E-mail: simone.palamara@polimi.it

the endocardium. In healthy propagation, the electrical signal coming from the atrioventricular (AV) node spreads rapidly into the PF and enters the ventricular wall at certain insertion sites, called Purkinje muscle junctions (PMJ) [2]. From these sites, the depolarization wave propagates into the myocardium, allowing for the ventricular excitation and contraction thanks to the activation of the cardiac muscle cells [3].

Computational models of cardiac electrophysiology can predict the electrical activity in the ventricles, and this can be an asset to clinicians in their diagnoses [4, 5] and selection of a therapy [6, 7]. The inclusion of PF in such models is therefore essential to simulate the ventricular excitation. This has been performed so far with surrogate models, based on space dependent conduction velocities [7], or by introducing sparse endocardial sources [8], or even by explicitly building a (non-patient-specific) network [9–13].

In [14], we presented a computational strategy for the generation of a patient-specific Purkinje network in the case of healthy electrical propagation. This method exploits available clinical data consisting in the activation times in some points of the endocardium of the left ventricle, trying to locate the PMJ so as to improve the accordance with these data. In [14], we showed the consistency and robustness of this methodology with respect to noisy data and different initial networks, while in [15], this strategy has been successfully applied to real healthy cases, highlighting the improvement of the accuracy obtained by using a patient-specific network with respect to the other models proposed in the literature. These works clearly show that the PF play a central role in the description of the electrical propagation.

In this paper, we extended the algorithm proposed in [14] for the generation of patient-specific Purkinje networks to the case of clinical data related to pathological propagations. This extension allowed us to apply our algorithm to patients affected by conduction disturbances. In particular, we considered clinical data acquired on three subjects, one characterized by the presence of scar tissue due to an old myocardial infarction and two suffering from the Wolff–Parkinson–White (WPW) syndrome. To assess the accuracy of the proposed method, we compared the results obtained by using the patient-specific networks with the ones obtained with a network generated without the clinical data. The results showed the applicability and reliability of our method also in pathological cases and the improved accuracy with respect to non-patient-specific networks, thus highlighting the essential role played by patient-specific networks in computational models to obtain an accurate description of the electrical activation in the left ventricle.

2. METHODS

2.1. Patient-specific clinical measurements

2.1.1. Description of the patients. Three patients have been considered in this study:

- subject 1, a 66-year-old individual with an old myocardial infarction and a characteristic apical aneurysm. She or he is characterized by an enlargement of the left ventricular chamber, due to a previous myocardial infarction at the apex with a resultant scar formation and a loss of contractile function leading to a chamber dilation;
- subjects 2 and 3, a 46-year-old individual and a 45-year-old individual suffering from a muscular pre-excitation, the WPW syndrome, given by the presence of an anomalous pathway, the bundle of Kent, between the left atrium and the left ventricle, in absence of any structural heart disease.

2.1.2. Acquisition of imaging data and reconstruction of the ventricular geometry. Subject 1 underwent an X-ray computed tomography acquired with a Philips (Eindhoven, Netherlands) CT scanner with 237 slices, with 512×512 pixels and voxel size equal to $0.429 \times 0.429 \times 0.7$ mm^3. Subjects 2 and 3 underwent a non-contrast enhanced 3D whole heart sequence, cardiac and respiratory gated, performed with a 1.5-Tesla MRI Unit (Magnetom Avanto, Siemens Medical Systems, Erlangen, Germany) and an eight-channel phased array torso coil. The following parameters have been used: voxel resolution $= 1.7 \times 1.6 \times 1.3$ mm^3; TE (echo time) $= 1.46$ ms; TR (repeti-

tion time) = 269.46 ms; slice thickness = 1.3 mm with 104 slices per single slab; acquisition matrix = 256×173; flip angle = 90°.

A manual segmentation of such geometries has been made by using the software ITK-SNAP (Paul A. Yushkevich, Philadelphia, Pennsylvania, United States; Hui Zhang, Philadelphia, Pennsylvania, United States) 2.4.0 [16].

2.1.3. Acquisition of electrical data. The activation time is defined as the time difference between a selected point on the body-surface electrocardiogram (ECG) and the time of steepest negative intrinsic deflection in the intracardiac electrogram measured by a mapping catheter, which is taken as indicator that the activation front has reached the underlying muscle. The Ensite NavX system is capable of accurately locating any electrode catheter within a 3D navigation field, allowing for the reconstruction of the heart geometry and providing accurate, real-time catheter navigation to obtain the maps of activation times. This system consists of three pairs of patches placed on the body surface in orthogonal axes. A low power electrical potential is generated across each pair of patches generating the three-dimensional navigation field. The system measures the local voltage of any electrode and is able to separate the component due to the navigation field, which gives the position of the electrode catheter, from the cardiac electrical potential, which allows to compute the activation time in the point at hand. The EnSite NavX technology provides an algorithm for compensation of catheter shifts due to respiratory motion, based on the identification of breathing-dependent changes of transthoracic impedances. In [17], it has been shown through *in vivo* experiments that this system enables accurate and reproducible real-time localization of electrode positions with a precision of 0.7 ± 1.5 mm, whereas in [18], it has been shown that this system does not distort the quality of the local ECG. For further details on the EnSite NavX system, we refer the reader to [19, 20].

A bi-ventricular mapping of the endocardium has been performed for all the three subjects by means of the Ensite NavX system, and only the information on the left ventricle has been considered. To this aim, a 7-Fr deflectable electro-catheter has been inserted through the right femoral artery with a retrograde trans-aortic approach (Medtronic Enhancr II 5523/Medtronic Conductr) (Minneapolis, Minnesota, United States). For the three subjects, we acquired electrical maps consisting in 193, 141, and 100 measures, respectively.

In what follows, let $\mathcal{I} := \{\boldsymbol{x}_i \in \Omega_e,\ i = 1, \ldots, N\}$ be the set of points where the measures have been acquired, T_i the corresponding measured activation times, and Ω_e the endocardium domain.

2.2. Modeling the electrical activation

The algorithm for the generation of the patient-specific Purkinje network proposed in this work is based on the computation of the discrepancy between measured and computed activation times. The latter are obtained by suitable mathematical models describing the electrical activation in the muscle and in the Purkinje network. More precisely, we considered the *eikonal equation* to describe both muscle and Purkinje network electrical activation.

2.2.1. Activation in the muscle. The activation times in the muscle could be obtained by solving mathematical models for the tissue electrophysiology, such as the *bidomain* and *monodomain* ones [21–24], consisting in modeling the ventricular tissue as a functional syncytium of electrically coupled cells and in deriving continuous models for the ionic currents. Such models allow us to compute the transmembrane potential in each point of the muscle by solving a time-dependent problem and thus to recover the related activation times.

In this work, we considered a simplified model, the *anisotropic eikonal equation* [25, 26], which describes directly the activation times in any point of the muscle. This is a steady problem, far less expensive in terms of computational time than the bidomain and monodomain ones. However, it provides only the activation times of the cardiac tissue and does not describe the cellular dynamics. This prevents the application of the eikonal model to the study of phenomena such as re-entries or arrhythmias. Additionally, the eikonal model does not take into account the effects of wave-front curvature, or the interaction between a wave-front with the domain boundaries or with other fronts. Nevertheless, the eikonal model has been proved to be a good approximation of the bidomain one

[25] if we are interested only in the activation times, and, for this reason, it has been used also for clinical applications [27].

Let Ω_m be the myocardial domain and $u_m = u_m(\boldsymbol{x})$ the unknown activation time. Then, the anisotropic eikonal model reads

$$\begin{cases} V_f \sqrt{(\nabla u_m)^T \, D \, \nabla u_m} = 1 & \boldsymbol{x} \in \Omega_m, \\ u_m(\boldsymbol{x}) = u_{m,0}(\boldsymbol{x}) & \boldsymbol{x} \in \Gamma_m, \end{cases} \tag{1}$$

where $D = D(\boldsymbol{x}) \in \mathbb{R}^{3\times 3}$ is the anisotropic tensor accounting for the orientation of the muscular fibers, $V_f = V_f(\boldsymbol{x})$ is the conduction velocity along the fibers, Γ_m is the set of boundary points generating the front, and $u_{m,0}(\boldsymbol{x})$ is the value of the activation time on Γ_m. For the anisotropic tensor, we used the following expression: [25]

$$D(\boldsymbol{x}) = k^2 \boldsymbol{I} + (1 - k^2)\boldsymbol{a}(\boldsymbol{x})\boldsymbol{a}(\boldsymbol{x})^T, \tag{2}$$

where k is the ratio between the conduction velocities in the orthogonal and longitudinal directions with respect to the fibers and $\boldsymbol{a}$ is the unit vector tangential to the fibers.

To generate the muscular fibers in our real geometries, we used the strategy proposed in [28], which produces a uniform transmural variation of the fiber direction. This method is based on the identification of three orthogonal directions for each point of the domain, the first one determined by solving a harmonic problem, the second one aligned with the longitudinal ventricular axis, and the third one determined so to guarantee mutual orthogonality.

2.2.2. Activation in the Purkinje network. To solve problem (1), we need to provide suitable boundary conditions on Γ_m. In a normal propagation, Γ_m coincide with the PMJ, because the signal traveling along the Purkinje network enters the muscle through these junctions. In an anomalous propagation, additional sources could be present, for example, given by fronts that originated from the intramyocardial region. In any case, we need to introduce a mathematical model for the description of the activation in the Purkinje network. To this aim, we considered the 1D eikonal equation, because we were interested in computing only the activation times in the network (in particular at the PMJ).

Let Ω_p be the one-dimensional Purkinje network and $u_p = u_p(\boldsymbol{x})$ the unknown activation time in the network. Then, the eikonal model reads

$$\begin{cases} V_p \left| \dfrac{\partial u_p}{\partial s} \right| = 1 & \boldsymbol{x} \in \Omega_p, \\ u_p(\boldsymbol{x}) = u_{p,0}(\boldsymbol{x}) & \boldsymbol{x} \in \Gamma_p, \end{cases} \tag{3}$$

where $V_p = V_p(\boldsymbol{x})$ is the conduction velocity (5–10 times greater than the muscular one [29]), s is the curvilinear coordinate along the network, Γ_p is the set of points generating the front in the network (e.g., in a normal propagation, the AV node), and $u_{p,0}(\boldsymbol{x})$ is the value of the activation time on Γ_p.

2.3. The solution of the coupled network/muscle problem

The PF form a subendocardial network characterized by a high conduction velocity V_p (3–4 m/s) and are isolated from the muscle, except at their endpoints, the PMJ, which are located on the endocardium. In a normal electrical propagation, the signal originates at the AV node and then spreads into the Purkinje network. Once the electrical signal has reached the PMJ, it enters the ventricle with a delay d_o of about 10–15 ms [10, 30], and then it propagates into the ventricular muscle, with a slower conduction velocity V_f (0.3–1 m/s) (*orthodromic propagation*).

In some pathological cases characterized by disturbances in the electrical propagation, it is important to consider also the propagation from the muscle toward the PF, owing to muscular intramyocardial sources, as it happens, for example, in a premature muscular activation or in a branch block (*antidromic propagation*; see, e.g., [31]). In this case, the signal enters the network at the PMJ with a delay d_a of about 2–3 ms [10] and then propagates backward into the network. Thus,

in general, the electrical propagation is characterized by two fronts, one originating at the AV node and one at the intramyocardial sources, leading to a coupled problem. This allows us to distinguish between two kinds of PMJ, those activated by the AV node or by other PMJ (*orthodromic PMJ*) and those activated by the muscular sources (*antidromic PMJ*). We observe that the antidromic PMJ could not activate the muscle (and thus any measurement points). Indeed, these PMJ are activated by the muscular front, and, owing to the antidromic delay, they are not able to generate a front that reaches the muscle before the muscular front itself.

Algorithm 1 *Solution of the coupled network/muscle problem (1)–(3)*

1. Solve the 1D eikonal problem $(3)_1$ in the network with the following boundary condition

$$u_{p,AV}(\boldsymbol{x}) = u_{p,AV,0}(\boldsymbol{x}) \quad \boldsymbol{x} \in \Gamma_{p,AV},$$

   where $\Gamma_{p,AV}$ identifies the AV node and with $u_{p,AV,0}$ given, thus determining the activation times $u_{p,AV}$ in the network if only the AV node was considered as source;
2. Solve the 3D eikonal problem $(1)_1$ in the myocardium with the following boundary condition

$$u_{m,m}(\boldsymbol{x}) = u_{m,m,0}(\boldsymbol{x}) \quad \boldsymbol{x} \in \Gamma_{m,m},$$

   with $u_{m,m,0}$ given, thus determining the activation times $u_{m,m}$ in the muscle if only the muscular sources were considered;
3. Given the set of the locations of the PMJ $\mathcal{P} = \{\boldsymbol{y}_j,\ j = 1, \ldots, M\}$, we split $\mathcal{P}$ in two subsets $\mathcal{P}_o$ and $\mathcal{P}_a$ defined as follows: in $\mathcal{P}_a$ we include the locations of the PMJ which satisfy

$$u_{m,m}(\boldsymbol{y}_j) + d_a \leqslant u_{p,AV}(\boldsymbol{y}_j) + d_o,$$

   that is those activated by the muscular front (antidromic PMJ), whereas in $\mathcal{P}_o$ we include the locations of the remaining PMJ, that is those activated by the network (orthodromic PMJ, see Figure 1, left);
4. Solve the 1D eikonal problem $(3)_1$ in the network with the following boundary conditions

$$\begin{cases} u_{p,AV-a}(\boldsymbol{x}) = u_{p,AV,0}(\boldsymbol{x}) & \boldsymbol{x} \in \Gamma_{p,AV}, \\ u_{p,AV-a}(\boldsymbol{y}_j) = u_{m,m}(\boldsymbol{y}_j) + d_a & \boldsymbol{y}_j \in \mathcal{P}_a, \end{cases} \tag{4}$$

   thus determining the activation times $u_{p,AV-a}$ in the network generated by the AV node and by the antidromic PMJ;
5. Identify which orthodromic PMJ are activated by the AV node and which ones are activated by an antidromic PMJ, thus generating the subsets $\mathcal{P}_{o-AV}$ and $\mathcal{P}_{o-a}$ (see Figure 1, left);
6. Solve the 3D eikonal problem (1) in the muscle with the following boundary conditions

$$\begin{cases} u_{m,m-o}(\boldsymbol{x}) = u_{m,m,0}(\boldsymbol{x}) & \boldsymbol{x} \in \Gamma_{m,m}, \\ u_{m,m-o}(\boldsymbol{y}_j) = u_{p,AV-a}(\boldsymbol{y}_j) + d_o & \boldsymbol{y}_j \in \mathcal{P}_o, \end{cases} \tag{5}$$

   thus determining the activation times $u_{m,m-o}$ in the muscle generated by the muscular sources and by the orthodromic PMJ;
7. Identify the orthodromic PMJ which activate at least a measurement point, thus generating the subset $\mathcal{P}_{o-active}$ (orthodromic/active PMJ). Notice that in general we have $\mathcal{P}_{o-AV} \cap \mathcal{P}_{o-active} \neq \varnothing$ and $\mathcal{P}_{o-a} \cap \mathcal{P}_{o-active} \neq \varnothing$. We call $\mathcal{I}_o$ the subset of $\mathcal{I}$ of the measurement points $\boldsymbol{x}_i$ activated by the orthodromic/active PMJ (that is the ones belonging to $\mathcal{P}_o \cap \mathcal{P}_{o-active}$), and $\mathcal{I}_{o-a}$ the subset of $\mathcal{I}_o$ of the measurement points $\boldsymbol{x}_i$ activated by the orthodromic/active PMJ belonging to $\mathcal{P}_{o-a} \cap \mathcal{P}_{o-active}$;
8. Set $u_m = u_{m,m-o}$ and $u_p = u_{p,AV-a}$.

To solve the coupled problem given by (1) and (3) accounting for possible antidromic propagations, we proceeded as follows. Let $\Gamma_{m,m} \subset \Gamma_m$ be the subset of all boundary sources for problem (1) located in the muscle domain. Of course, $\Gamma_m \setminus \Gamma_{m,m}$ coincides with the set of all the orthodromic PMJ.

We made the following assumption:

H. The antidromic activation of the PMJ is produced only by the muscular sources.

The previous hypothesis states that the only muscular pathways that activate the network are generated by the muscular sources. In other words, a signal that starts from the AV node and enters the muscle through a PMJ cannot re-enter the network. In this context, we considered Algorithm 1.

Hypothesis H allows us to avoid subiterations in Algorithm 1. Of course, it provides a simplification, because it does not allow for re-entries in the network. Owing to the high values of the delays d_o and d_a, it is reasonable to assume that for healthy PF, the phenomenon of the re-entry does not significantly influence the solution of the coupled problem. However, this is an interesting point and will be the subject of future works.

To summarize, referring to the notation introduced in Algorithm 1, we have the following sources:

- the AV node, which activates the orthodromic PMJ belonging to $\mathcal{P}_{o-AV}$;
- the orthodromic PMJ activated by the AV node (belonging to $\mathcal{P}_{o-AV}$), which activates the myocardium and thus, possibly, some measurement points;
- the orthodromic PMJ activated by the antidromic PMJ (belonging to $\mathcal{P}_{o-a}$), which activates the myocardium and thus, possibly, the measurement points belonging to $\mathcal{I}_{o-a}$;
- the antidromic PMJ (belonging to $\mathcal{P}_a$), which are all activated by the muscular sources and activate the orthodromic PMJ belonging to $\mathcal{P}_{o-a}$;
- the muscular sources, which activate the myocardium (and thus, possibly, some measurement points) and the antidromic PMJ.

2.4. Patient-specific generation of the Purkinje fibers

In this section, we describe the algorithm for the generation of a patient-specific network, which is in fact an extension of the one proposed in [14] to treat also pathological cases. The principal idea consists in starting from an initial network (*generic network*), and in adapting the locations of the PMJ so as to minimize the discrepancy with the clinical measurements. In particular, the key point is to separate the antidromic PMJ from the orthodromic ones. Indeed, the antidromic PMJ are boundary sources for the network, thus possibly having a global influence in the activation times in the network, whereas the orthodromic PMJ are boundary sources for the muscle activation. For this reason, we first adapt the locations of the antidromic PMJ, and then the ones of the orthodromic PMJ.

We observe that to adapt the location of the antidromic PMJ, it is necessary to introduce some new steps with respect to the algorithm proposed in [14], because in that work we dealt only with a normal electrical propagation, where antidromic PMJ are absent. On the contrary, to adapt the orthodromic PMJ, we follow the steps reported in [14], so that for further details on this point, we refer the reader to that work.

To describe the Purkinje network, we consider several levels of generation, where *active branches* and *leaves* could be identified. An active branch can generate other branches, whereas leaves terminate at their end points, which are identified with the PMJ. In particular, the leaves S_j, $j = 1, \ldots, M$, start from the base $\boldsymbol{w}_j$ and terminate at the PMJ P_j; see Figure 1, right.

2.4.1. Generation of the generic network. To generate the generic network, we proceeded as in [14], following the proposals provided in [9, 11, 32], based on the introduction of a fractal rule, namely the 'Y' production rule. In particular, first, we manually design the bundle of His and the main bundle branches, according to anatomical a priori knowledge. Then, we generate the leaves by means of a Bernoullian probability law with probability $p = \sqrt{l/M_{lev}}$, where l is the current level and M_{lev} the maximum number of levels allowed. Moreover, the lengths of the left and right branches L_l and L_r, and the branching angle α (that is, the angle between two new branches)

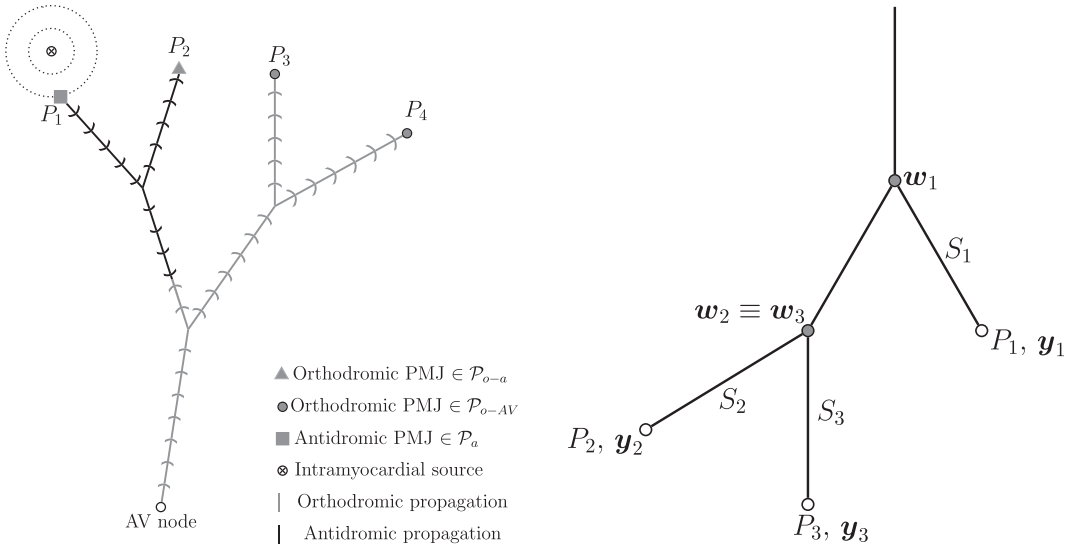

Figure 1. On the left: classification of the PMJ. On the right: structure of the Purkinje network, with the bases $\boldsymbol{w}_k$, the leaves S_k, and the PMJ P_k. In the picture, we have $M = 3$.

are described by Gaussian variables. This allowed to generate a generic Purkinje network $\mathcal{N}^{(0)}$, characterized by $M^{(0)}$ leaves S_j and PMJ P_j.

The idea is now to locate the PMJ so as to maximize the accordance with the endocardial measures. A datum T_i located at $\boldsymbol{x}_i$ is said to be *satisfied* if

$$|\eta_i| \leqslant \varepsilon, \tag{6}$$

where

$$\eta_i := \frac{t_i - T_i}{|T_i|},\ i = 1, \ldots, N, \tag{7}$$

and $t_i := u_m(\boldsymbol{x}_i)$, $i = 1, \ldots, N$, are the activation times computed at the measurement points by solving the coupled problem (1)–(3).

2.4.2. Classification of the PMJ. We first need to detect which are the orthodromic and antidromic PMJ of the generic network. To this aim, we solve Algorithm 1 with this network. This allows us to generate the subsets $\mathcal{P}_a^{(0)}$, $\mathcal{P}_{o-AV}^{(0)}$, and $\mathcal{P}_{o-a}^{(0)}$ and to compute the activation times $u_m^{(0)}$ and $u_p^{(0)}$ in all the points of $\Omega_m \cup \Omega_p$, in particular at the PMJ and at the measurement points $\boldsymbol{x}_i$.

2.4.3. Move or delete the antidromic PMJ. In order to improve the accordance of the computed activation times $t_i^{(0)}$ with the measurements T_i, we start moving the antidromic PMJ. We observe that the antidromic PMJ do not activate directly the measurement points, but they have an influence on those belonging to $\mathcal{I}_{o-a}$ through the orthodromic PMJ belonging to $\mathcal{P}_{o-a}^{(0)} \cap \mathcal{P}_{o-active}^{(0)}$. In particular, we want to avoid that the signal reaches the measurement points too early, because this would prevent to move other PMJ and to reduce the discrepancy with the measures. So, we move the antidromic PMJ such that all the measurements indirectly activated by an antidromic PMJ are either satisfied or late.

The movement of an antidromic PMJ is based on an iterative procedure. In particular, at each iteration, we identify the measurement point $\boldsymbol{x}_i \in \mathcal{I}_{o-a}$ with the smallest and negative η_i, and we move the PMJ belonging to $\mathcal{P}_a$, which, through an orthodromic/active PMJ, activates $\boldsymbol{x}_i$. To this aim, at each iteration $k = 1, \ldots, K_1$, we compute for each measurement point belonging to $\mathcal{I}_{o-a}$ the

discrepancies (7), and then we take its minimum $\delta^{(k)}$. Now, if $\delta^{(k)} > -\varepsilon$, with ε a given tolerance, then we stop the iterations without any further modification of the network $\mathcal{N}^{(k-1)}$, because all the measurements points activated by the PMJ belonging to $\mathcal{P}_{o-a}^{(k-1)} \cap \mathcal{P}_{o-active}^{(k-1)}$ are accurately satisfied or late. On the contrary, if $\delta^{(k)} < -\varepsilon$, we move the antidromic PMJ P_j, which is responsible, through an orthodromic/active PMJ, of the premature activation in $\boldsymbol{x}_i$. In particular, we locate P_j on the geodesic line $r^{(k)}$ joining the muscular source, which activated P_j and the base $\boldsymbol{w}_j$ of the leaf ending with P_j, so as to satisfy the measurement $\boldsymbol{x}_i$. To this aim, let τ be the activation time at the base $\boldsymbol{w}_j$ due to the 1D eikonal problem in the network. To avoid P_j from producing a signal that is too early in $\boldsymbol{x}_i$, we would like the activation time in $\boldsymbol{w}_j$ to be as close as possible to $\tau - \delta^{(k)} T_i$. Indeed, if the activation time in $\boldsymbol{w}_j$ was exactly $\tau - \delta^{(k)} T_i$, then the point $\boldsymbol{x}_i$ would be activated precisely at time T_i, thus producing a zero error. Therefore, we move P_j in the point $\boldsymbol{y}_j^{(k)}$ on $r^{(k)}$ such that the quantity

$$\left| \left(\tau - \delta^{(k)} T_i \right) - \left(u_{m,m} \left(\boldsymbol{y}_j^{(k)} \right) + d_a + l^{(k)} / V_p \right) \right|$$

is minimal, provided that

$$\frac{\left| \left(\tau - \delta^{(k)} T_i \right) - \left(u_{m,m} \left(\boldsymbol{y}_j^{(k)} \right) + d_a + l^{(k)} / V_p \right) \right|}{T_i} < \varepsilon.$$

Here, $l^{(k)}$ is the distance between $\boldsymbol{y}_j^{(k)}$ and $\boldsymbol{w}_j$, so that $(u_{m,m}(\boldsymbol{y}_j^{(k)}) + d_a + l^{(k)}/V_p)$ is the activation time at the base $\boldsymbol{w}_j$ after the movement of P_j (Figure 2).

Otherwise, if

$$\frac{\left| \left(\tau^{(k)} - \delta^{(k)} T_i \right) - \left(u_{m,m} \left(\boldsymbol{y}_j^{(k)} \right) + d_a + l^{(k)} / V_p \right) \right|}{T_i} \geqslant \varepsilon$$

for any point on $r^{(k)}$, then we eliminate P_j. This allows us to produce in any case a new network $\mathcal{N}^{(k)}$ and to compute the new activation times $u_m^{(k)}$ in all the myocardium by solving Algorithm 1. At the end of this procedure, if we have performed K_1 iterations, we have generated the network $\mathcal{N}^{(K_1)}$.

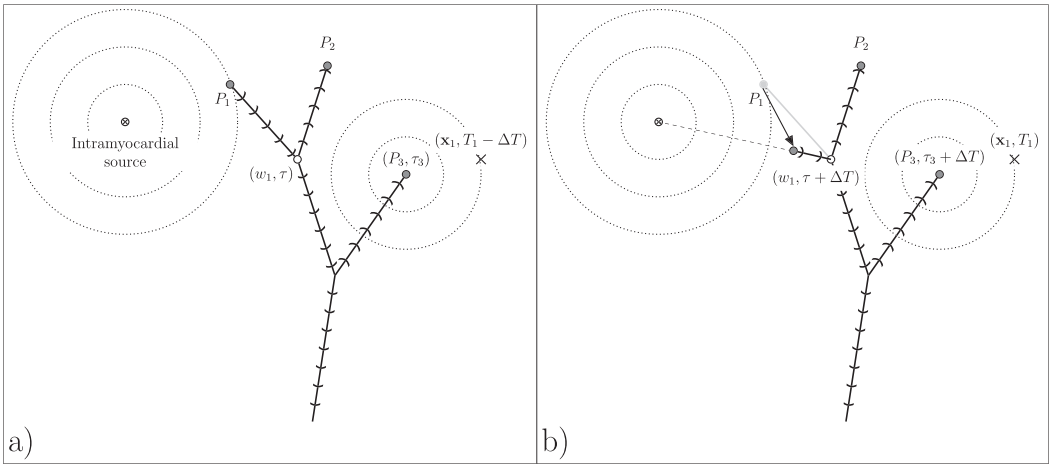

Figure 2. Sketch of the antidromic moving procedure. On the left: the signal reaches the measurement point $\boldsymbol{x}_1$ earlier at time $T_1 - \Delta T$. On the right: after the movement of the PMJ P_1, the signal reaches the base w_1, the PMJ P_3 and the measurement point $\boldsymbol{x}_1$ with a delay of ΔT, thus guaranteeing the satisfaction of the datum T_1.

2.4.4. Construction of the regions of influence. We are now ready to adapt the location of the orthodromic PMJ. To this aim, we say that a set of M sources (z_k, ζ_k) is *compatible* with the measurements if the following holds:

$$u_m(\boldsymbol{x}_i) = T_i \qquad \forall\, i = 1, \ldots, N, \tag{8}$$

with

$$\begin{cases} V_f \sqrt{(\nabla u_m)^T\, D\, \nabla u_m} = 1 & \boldsymbol{x} \in \Omega_m, \\ u_m(z_k) = \zeta_k & k = 1, \ldots, M. \end{cases} \tag{9}$$

Following [14], to identify possible compatible sources, we consider the following *backward eikonal problem* in the unknown $\tilde{u}_m$:

$$\begin{cases} V_f \sqrt{(\nabla \tilde{u}_m)^T\, D\, \nabla \tilde{u}_m} = 1 & \boldsymbol{x} \in \Omega_m, \\ \tilde{u}_m(\boldsymbol{x}_i) = -T_i & i = 1, \ldots, N. \end{cases} \tag{10}$$

The solution of such a problem divides the domain Ω_m into N regions R_i, called *regions of influence*, which associate to each point $\boldsymbol{x}_i$, where the measurements are available, the points of the myocardium which possibly activate $\boldsymbol{x}_i$ at time T_i, if used as source points for the muscular propagation. In particular, the boundaries of the regions R_i are identified by the points of collision of two or more fronts propagating from the measurement points $\boldsymbol{x}_i$ (see Figure 3 for the case $N = 3$).

Exploiting the function $\tilde{u}_m$, we are now able to build a set of M sources that is compatible with the measures. Indeed, let $\hat{z}_1, \ldots, \hat{z}_M$ be M points such that at least one point falls in each region R_i or its boundary. Moreover, set

$$\hat{\zeta}_k := -\tilde{u}_m(\hat{z}_k),\ k = 1, \ldots, M. \tag{11}$$

Then, we have the following result.

Proposition 1
The M sources $(\hat{z}_k, \hat{\zeta}_k)$, $k = 1, \ldots, M$, with the $\hat{\zeta}_k$'s defined by (10)–(11), are compatible with the measures $(\boldsymbol{x}_i, T_i)$, $i = 1, \ldots, N$, that is, they satisfy (8)–(9).

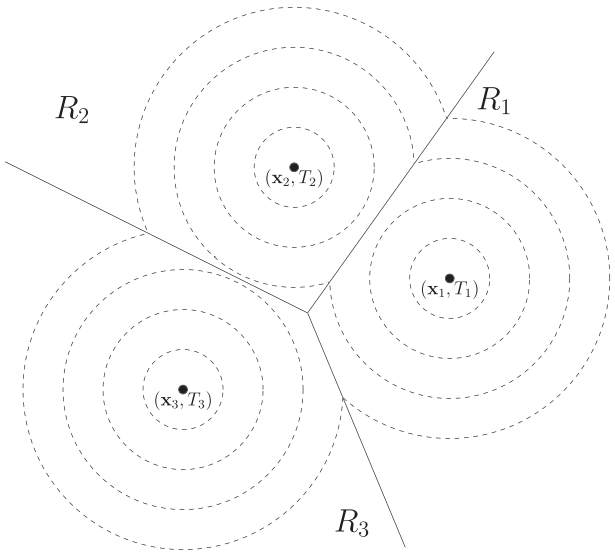

Figure 3. Regions of influence. Representation of the contour lines of a possible solution of (10) with $N = 3$. The lines represent the points of collision among two or more fronts, and they divide the domain into three regions R_i, called regions of influence.

Proof
The proof is a trivial extension to the 3D case of the one given in [14] for endocardial propagations, provided that the Euclidean distance is replaced by the anisotropic metric induced by the muscular fibers. □

2.4.5. Move the orthodromic PMJ. This and the following step (delete and create orthodromic PMJ) are taken from [14], so that we refer the reader to that work for further details.

As this procedure is given by a single step, we drop here the iteration index. Let P_j be an orthodromic PMJ and N^o the number of measurement points belonging to $\mathcal{I}_o$, which is those activated by an orthodromic PMJ. We constrain the movement of an orthodromic PMJ to stay within its region of influence and to be relatively small so that the length of the modified branch is still in the physiological range. We want that conditions (6) possibly hold for all the measurement points belonging to $\mathcal{I}_o$. However, to check such conditions, one needs to solve a 3D anisotropic eikonal problem for each movement of a PMJ. To limit the solution of 3D problems, we decided to use the following discrepancies:

$$\chi_j^i := \frac{u_p\left(\mathbf{y}_j^i\right) + d_o - \left(-\tilde{u}_m\left(\mathbf{y}_j^i\right)\right)}{|T_i|}, \quad j = 1, \ldots, M_i,\ i = 1, \ldots, N, \tag{12}$$

where M_i is the number of PMJ belonging to the region of influence R_i and $\mathbf{y}_j^i$ is the location of the j-th PMJ belonging to R_i. The quantities χ_j^i measure the discrepancy between the activation time in a PMJ computed with the 1D eikonal problem in the network, and the solution of the 3D backward eikonal problem (normalized by the measure $|T_i|$). The use of these quantities instead of (7) has the advantage to use the solution of the backward problem, which has been already solved to identify the regions of influence. We have the following result:

Proposition 2
Let the following conditions hold for all the orthodromic PMJ:

(i) Each region of influence contains at least one orthodromic PMJ.
(ii) $|\chi_j^i| \leqslant \varepsilon$ for all the orthodromic PMJ.
(iii) $\min\limits_{i=1,\ldots,N^o}\left(\min\limits_{j=1,\ldots,M_i} \chi_j^i\,|T_i|\right) \geqslant -\varepsilon\, T_{min}$, where $T_{min} := \min\limits_{i=1,\ldots,N^o} |T_i|$.

Then conditions (6) are all satisfied, that is, $|\eta_i| \leqslant \varepsilon,\ i = 1, \ldots, N^o$.

Proof
The proof is the same of the one provided in [14], provided that the Euclidean distance is replaced by the anisotropic metric induced by the muscular fibers. □

All the PMJ such that $|\chi_j^i| > \varepsilon$ are now moved in order to improve the accordance with the clinical measures, guaranteeing, however, that new locations are compatible with the solution of the 1D eikonal problem in the Purkinje network. Assume that the orthodromic PMJ P_j needs to be moved and belongs to the region of influence R_i. We then decide to locate the PMJ on the geodesic line r joining the measure $\boldsymbol{x}_i$ and the base of the leaf ending at P_j. In particular, in analogy with the movement of the antidromic PMJ, we want that the activation time in the new PMJ due to network propagation is as close as possible to the one given by the backward 3D eikonal problem. To this aim, let τ be the activation time at the base $\boldsymbol{w}_j$ due to the 1D eikonal problem in the network. Then, we move P_j in the point $\boldsymbol{y}_j$ on r such that the quantity

$$|(\tau + l/V_p + d_o) + \tilde{u}_m(\boldsymbol{y}_j)|$$

is minimal, provided that

$$\frac{|(\tau + l/V_p + d_o) + \tilde{u}_m(\boldsymbol{y}_j)|}{T_i} < \varepsilon.$$

Here, l is the distance between $\boldsymbol{y}_j$ and $\boldsymbol{w}_j$, so that $\tau + l/V_p + d_o$ is the activation time at the new orthodromic PMJ P_j.

At the end of the moving procedure, we have obtained a new Purkinje network $\mathcal{N}^{(K_1+1)}$.

2.4.6. Delete and create orthodromic PMJ. Given a measurement point $\boldsymbol{x}_i$ activated by an orthodromic PMJ P_j, we have three cases:

- $\boldsymbol{x}_i$ is satisfied ($|\eta_i| < \varepsilon$).
- The signal generated from P_j reaches $\boldsymbol{x}_i$ in late ($\eta_i \geq \varepsilon$).
- The signal generated from P_j reaches $\boldsymbol{x}_i$ early ($\eta_i \leq -\varepsilon$).

As discussed in [14], in the third case, we have no possibility to satisfy the measure in $\boldsymbol{x}_i$ by creating new PMJ, whereas in the second case, the creation of new PMJ could satisfy the measure. For this reason, we delete the orthodromic PMJ P_j if $\eta_i \leq -\varepsilon$. On the contrary, if $\eta_i \geq \varepsilon$, we create a new orthodromic PMJ located on the geodesic line joining $\boldsymbol{x}_i$ with a suitable point of the portion of the network belonging to R_i (see [14] for further details).

After this procedure, we have obtained the final patient-specific Purkinje network $\mathcal{N}$.

We notice that the network generated by our method depends on the starting network and on some user parameters such as the mean value of the length and of the angles of the branches, the threshold to detect the satisfied points, and the conduction velocities. Once the initial network, the clinical measurements, and these parameters have been fixed, the solution produced by our methodology after the 'move' and 'delete' procedures is unique, in the sense that it generates always the same network. However, with the 'create' procedure, different networks could be generated, depending on the order used to go through the not satisfied points.

2.5. Description of the pathologies

In this section, we provide a brief description of the two pathologies considered in this work, and we point out how to adapt our algorithm to them.

2.5.1. The case of old myocardial infarction (subject 1). If no arrhythmia or electrical disease affecting the pathway of conduction is present (as what happened for subject 1), then all the PMJ are orthodromic so that all the sources of the muscular activation are given by the PMJ. Hence, we can apply our algorithm without the steps of moving and deleting antidromic PMJ, ending up with the algorithm presented in [14]. For this reason, for subject 1, it was enough to solve our method without the calibration of the antidromic PMJ, thus avoiding the solution of a coupled muscle/network problem. Moreover, as discussed in [14], the solution of a 2D isotropic eikonal problem, instead of an anisotropic 3D one, is enough in this case, because all the sources are located on the endocardium.

However, some remarks are in order. In particular, the myocardium of a patient with an old myocardial infarction is characterized by the presence of scar tissue, which replaces the healthy one in the region affected by the ischemic attack. This region is characterized by a reduced blood supply, resulting in the death of the muscular cells and thus in a progressive deterioration of the electrical activity. For this reason, the muscle is no longer excitable in the scar region, and then we imposed a zero conduction velocity on this portion of the endocardium [4] ($V_f = 0$). Moreover, we assumed that the ischemic attack affects also the conduction property of the Purkinje network located in the scar region. In particular, in this region, we set V_p about four times smaller than the physiological value, supposing that the signal propagates, even if slowly, also into the portion of PF belonging to the scar region [33]. We notice, however, that the state of the Purkinje system close to the scar region remains to be fully elucidated; in particular, it is still to be definitively proved that the PF have no access to the blood pool.

The location of the scar region for our computations has been estimated thanks to the electrical mapping, because the clinicians measured a null potential at the points belonging to the scar.

2.5.2. The case of the Wolff–Parkinson–White syndrome (subjects 2 and 3). The WPW syndrome is characterized by an accessory pathway between the left atrium and the left ventricle, named the bundle of Kent. In this case, we have a muscular intramyocardial source and therefore both orthodromic and antidromic PMJ, so that the complete algorithm presented in this work has been considered.

Observe that the clinical measures are all located on the endocardium, so that it was not possible to use the measures to locate the intramyocardial source. For this reason, the latter has been modeled as a single activation, located in the point that guaranteed the best accordance with the measures, among those where possibly the bundle of Kent enters the left ventricle.

3. RESULTS

In this section, we show the numerical results obtained by applying the strategy proposed in this work for the generation of a patient-specific Purkinje network for pathological cases. The aim is to compare the measured activation times with those obtained by using both the patient-specific network and the generic network.

First of all, we mention the boundary conditions that we have used for subjects 2 and 3 for the harmonic problem in the fibers generation (Section 2.2.1): we set an angle of $-75°$ at the endocardium and $+45°$ on the epicardium for subject 2, and $-60°$ at the endocardium and $+45°$ on the epicardium for subject 3 (an angle of $+90°$ corresponds to a fiber pointing toward the apex of the ventricle). In Figure 4, we reported the orientation of the muscular fibers obtained with this strategy in the case of subject 2. We remark that it was not necessary to describe the muscular fibers for subject 1, as explained in Section 2.5.1. Moreover, we imposed a time delay in the orthodromic propagation $d_o = 10$ ms for subject 1, and $d_o = 14$ ms for subjects 2 and 3, and a delay in the antidromic propagation $d_a = 3$ ms for subjects 2 and 3. Such values of the muscular fiber angles and of the delays have been chosen with a trial-and-error strategy to maximize the accordance with the clinical measures and are in the physiological ranges reported in [34] and [30], respectively. We remark that the results are quite independent of the value of the fiber angles prescribed at the boundaries, provided that they are chosen in the physiological ranges. Furthermore, the timing of the muscular source and of the AV node is chosen with a trial-and-error procedure to maximize the accordance of the results with the clinical measures.

For each of the three subjects, in Table I (first two rows), we reported the number of branches and PMJ for the generic and patient-specific networks, while in Figure 5, we depicted these networks.

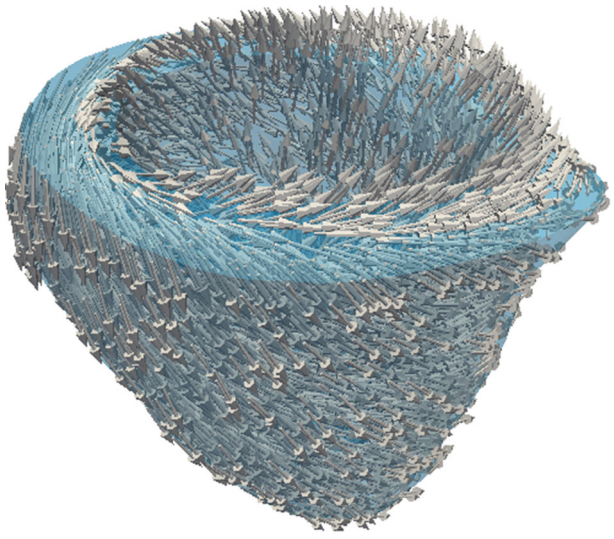

Figure 4. Muscular fibers orientation for subject 2.

Table I. Number of branches and PMJ, conduction velocities in the network (V_p), on the endocardium (V_e), along the muscular fiber (V_f) and transverse to the muscular fiber direction (V_t).

		Subject 1	Subject 2	Subject 3
Generic network	# branches	2144	1617	1493
	# PMJ	308	596	528
	V_p (m/s)	3.1	3.5	3.1
	V_e (m/s)	0.29	—	—
	V_f (m/s)	—	0.980	0.855
	V_t (m/s)	—	0.490	0.570
Patient-specific network	# branches	2047	1555	1404
	# PMJ	211	534	439
	V_p (m/s)	3.1	3.5	3.1
	V_e (m/s)	0.29	—	—
	V_f (m/s)	—	0.980	0.855
	V_t (m/s)	—	0.490	0.570

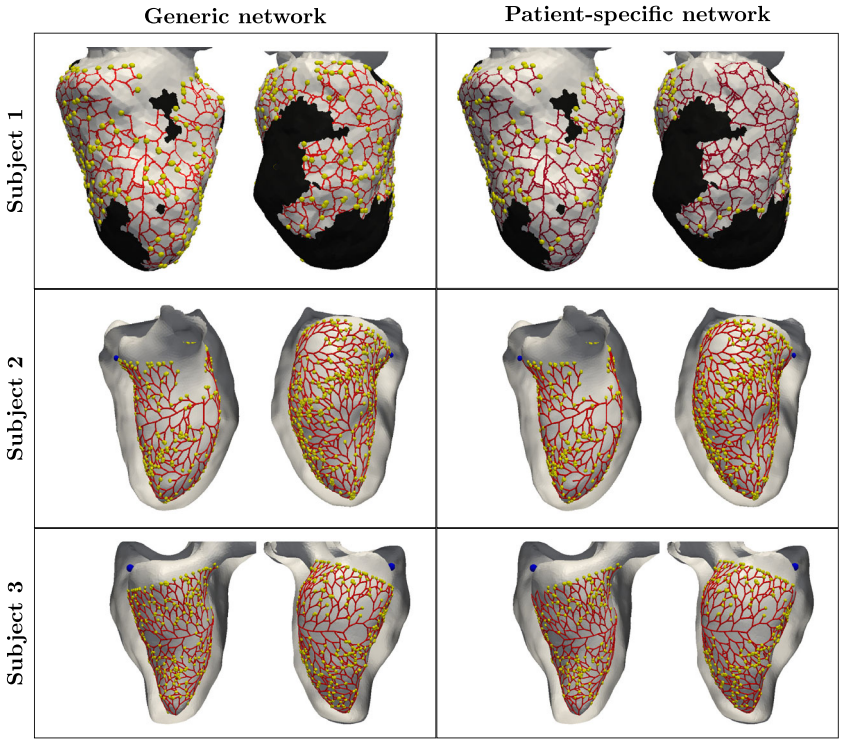

Figure 5. Generic networks (left), generated without any patient recorded data, and patient-specific networks (right), generated with the proposed algorithm by using clinical data. Each row represents a different subject. In yellow, we depicted the PMJ. For the first subject, we depicted only the endocardium, while for subjects 2 and 3, we depicted all the myocardium. For subject 1 (first row), we depicted in black the region of endocardium identified with the scar, and for subjects 2 and 3 (second and third rows), we depicted in blue the anomalous source due to the WPW syndrome.

To obtain the generic network, we used a mean value of branch length equal to 7.0 ± 0.3 mm for subject 1, the one with a dilated ventricle, and equal to 4.0 ± 0.3 mm for subjects 2 and 3, and a mean value of branch angle $60 \pm 1.8°$ for all the subjects. All these values fall in the physiological ranges proposed in [12].

The conduction velocities in the network (V_p), on the endocardium (V_e) for subject 1, along the muscular fiber direction (V_f) and transverse to the muscular fiber direction (V_t) for subjects 2 and

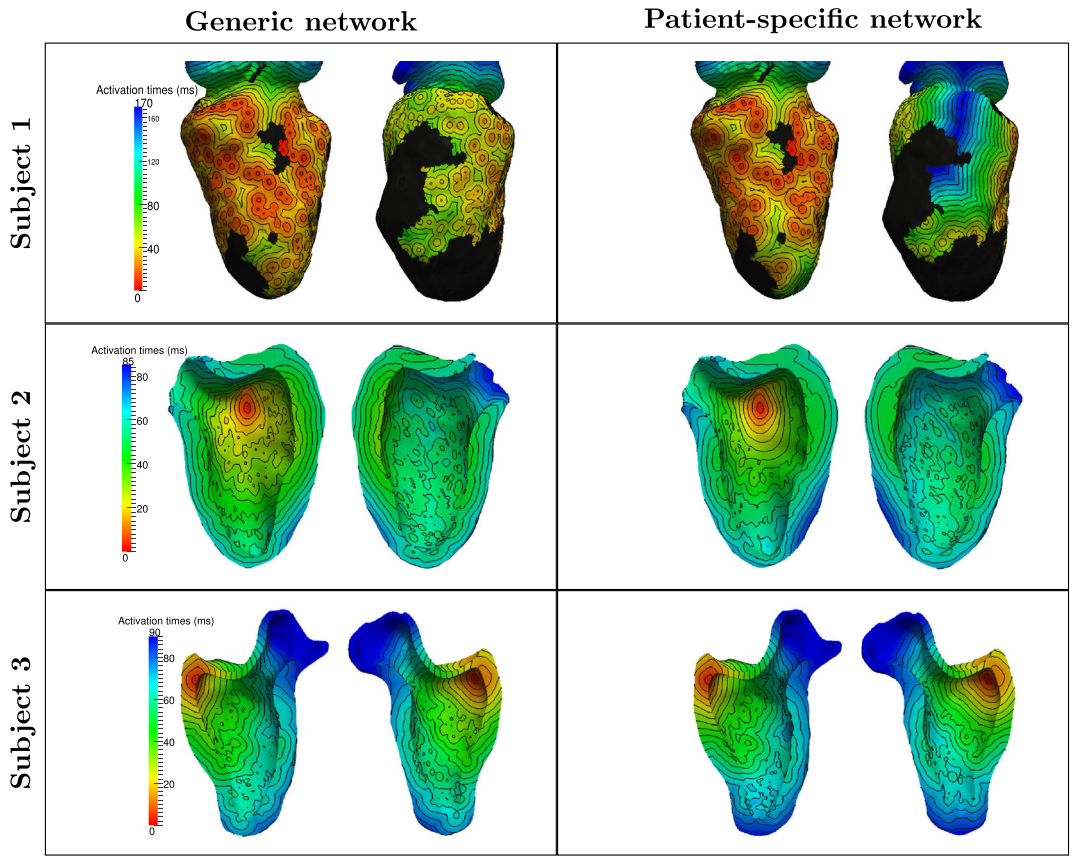

Figure 6. Computed activation times for the three subjects. Each row represents a different subject. Left: generic network, generated without any patient recorded data. Right: patient-specific network, generated with the proposed algorithm by using the clinical data.

3, have been tuned in order to maximize the accordance with the clinical measures with a trial-and-error strategy. We reported for all the subjects such quantities in Table I (third, fourth, fifth, and sixth rows). We notice that, for all the subjects, V_p falls in the physiological ranges 3.0–4.0 m/s, whereas for subject 1, V_e is slightly outside the physiological range 0.3–1.0 m/s [35]. Moreover, we notice that the value of the estimated velocity along the fibers direction V_f falls in the physiological range 0.6–1.0 m/s for both subjects 2 and 3 [29]. Finally, we notice that the estimated value of the velocities V_f and V_t satisfies, for both subjects 2 and 3, the physiological ratio $V_f / V_t \in (1.5, 2.0)$ [36]. Moreover, in all the simulations, the value of the tolerance ε was set equal to 0.15.

In order to assess the accuracy obtained by using the generated networks, for all the subjects, we performed a cross-validation test. In particular, we used 50% of the measures for the generation of the patient-specific network (training set), and the remaining measures to validate the networks (testing set).

In Figure 6, we show for the three subjects the activation times obtained by solving Algorithm 1 with the generic and patient-specific networks, whereas in Figure 7, we show the errors intended as the absolute values of the differences between the measured activation times in the testing sets and the corresponding computed data. Moreover, in Table II, we report the mean of these errors.

From these results, we observe that in all the cases, the use of the patient-specific network improved the accuracy with respect to the generic network. In particular, subject 1 highlighted a very large improvement, the mean error being halved when using the patient-specific network. Regarding subjects 2 and 3, we observe a lesser improvement in the accuracy when using the patient-specific network. This is probably strictly related to the WPW syndrome, as reported in Section 4.

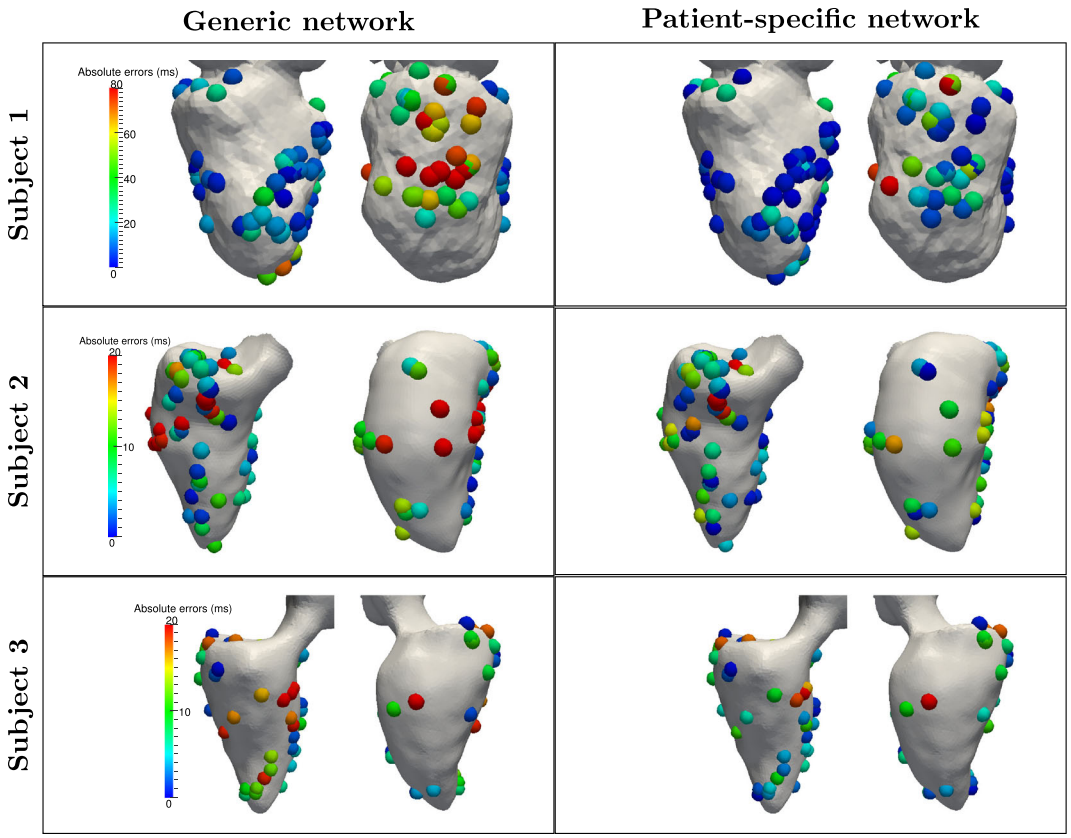

Figure 7. Errors between the measured activation times in the testing set and the corresponding computed data for the three subjects, represented by spheres located in the points where the measures have been acquired. Each row of the figure depicts the results of a subject obtained with the generic networks (left), generated without clinical data, and with the patient-specific networks (right), generated with the proposed methodology by using the clinical measures in the training set.

Table II. Mean errors (ms) for the three subjects in the case of the generic (top) and patient-specific (bottom) Purkinje networks.

	Subject 1	Subject 2	Subject 3
Generic network	30.57 ± 27.91	9.30 ± 7.29	10.11 ± 7.38
Patient-specific network	14.06 ± 15.52	7.16 ± 6.47	7.53 ± 6.30

To have a more accurate description of the error distribution, in Figure 8 (first row), we show for the three subjects the histograms representing the number of points N (over the total number) characterized by specific ranges of the error. These results confirmed the improvement in the accuracy obtained with the patient-specific networks. Again, we observed a significant improvement for subject 1 and a lesser improvement for subjects 2 and 3.

We observe that for subjects 2 and 3, the points of the endocardium could be activated either by the Purkinje network or by the underlying muscle owing to the anomalous pathway. Then, for such patients, we built the subset $\mathcal{K}$ of the testing set given by the measurement points activated in our simulations by the networks, and the subset $\mathcal{W}$ of the testing set given by the measurement points activated by the front propagating from the anomalous pathway. In Table III, we reported the mean errors related to each of these two subsets, whereas in Figure 8 (second row), we reported the corresponding histograms. These results clearly show that there is an appreciable improvement in the accuracy when using the patient-specific network for the measurement points activated by the PF

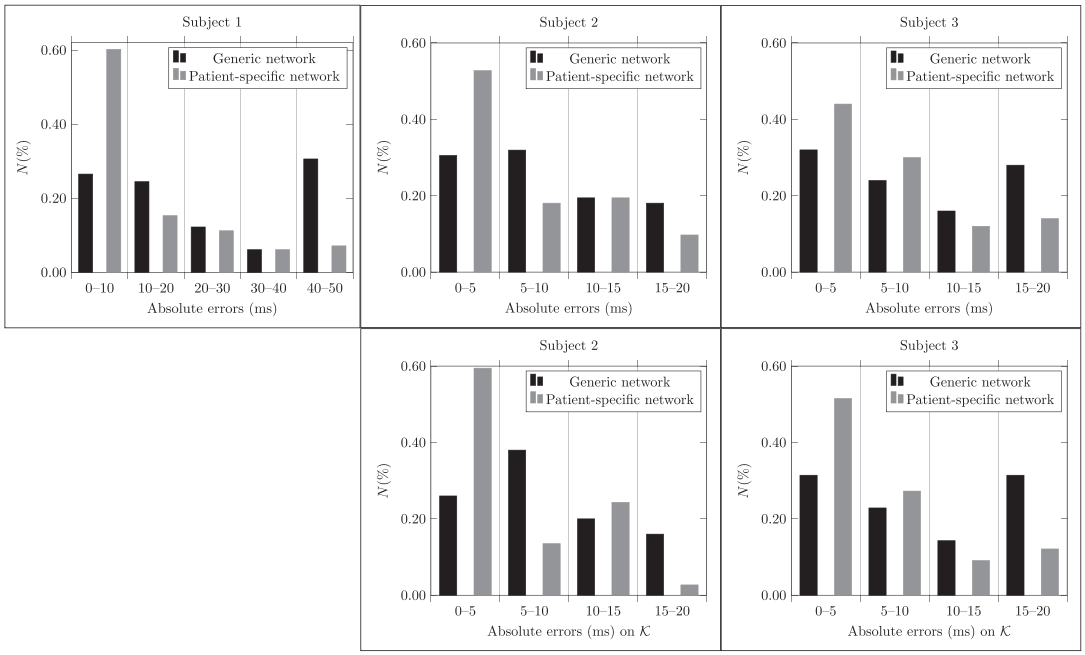

Figure 8. Histograms of the errors. From left to right, we reported the results for subjects 1, 2, and 3, respectively. In the second row, we reported for subjects 2 and 3 the histograms relative to the measurement points belonging to the subset $\mathcal{K}$.

Table III. Mean errors for the patients suffering from WPW on the subsets $\mathcal{K}$ and $\mathcal{W}$ in the case of the generic and patient-specific Purkinje networks.

	Network	Mean absolute error on $\mathcal{K}$ (ms)	Mean absolute error on $\mathcal{W}$ (ms)
Subject 2	Generic	9.09 ± 6.74	9.79 ± 8.38
	Patient specific	6.01 ± 5.00	8.38 ± 7.54
Subject 3	Generic	10.67 ± 7.47	8.82 ± 6.99
	Patient specific	6.95 ± 6.06	8.66 ± 6.60

(subset $\mathcal{K}$), whereas no significant improvements are observed for those activated by the anomalous signal (subset $\mathcal{W}$).

4. DISCUSSION

4.1. The case of old myocardial infarction

4.1.1. State of the art. The myocardial ischemia has been studied with computational models for over 20 years. The first computational models of this pathology studied the development of depressions in the ST segment of the ECG due to the developing of ischemic currents at the interface between damaged and healthy cells [37–39]. More recent studies investigated the possibility to recover information on the size and location of the ischemic region from such depressions by solving an inverse problem [5, 40]. The ischemic currents are developed during the plateau phase of the cell electrical activity, when all the muscle heart cells have been already activated. For this reason, the presence of the Purkinje network in these works has been neglected. Instead, if we are interested in modeling the ventricular activation to recover the QRS complex, it is mandatory to model the presence of the Purkinje network [33, 41]. As far as we know, the only work that included a (non-patient-specific) Purkinje network for the study of the ischemia is [10], where the authors studied the effect of such a network on the propagation of arrhythmias. Instead, in [3, 42], surrogate models of the PF have been considered, by using a variable-in-space conduction velocity on the endocardium.

4.1.2. Discussion of the results. The results reported in Figures 7 and 8 and in Table II for subject 1 clearly show the big improvement when the patient-specific network is used to compute the activation times on the endocardium. In particular, the mean error decreased by 54.0% with respect to the one obtained with the generic network, with over 60% of the measures characterized by an error less than 10 ms. Moreover, we observe the lack of PMJ in the patient-specific Purkinje network in the region opposite to the septum, just between the two big scar regions (Figure 5, first row on the right). This probably reflects the fact that the Purkinje network is in fact a little bit damaged in that region, owing to the vicinity of the infarction. Of course, the generic network is not able to recognize such a damaged region, because it localizes the PMJ randomly. Accordingly, looking at Figure 6 (first row), we can appreciate the differences between the two networks in the activation pattern in the region opposite to the septum, leading to different values of the errors in this region, as shown in Figure 7.

These results showed that our approach could be used successfully in presence of a muscular conduction damage and that it is able to capture the specificity of the patient at hand.

4.2. The case of the Wolff–Parkinson–White syndrome

4.2.1. State of the art. The WPW syndrome often leads to supraventricular tachycardia that needs to be treated with an ablation therapy [43]. Computational studies related to this pathology can be found in [44], where a model of the WPW has been presented with the aim of analyzing the relation between the location of the intramyocardial pathway and the wave form of the ECG, and in [45], where the development of supraventricular tachycardia as a consequence of WPW has been investigated. In both papers, simplified non-patient-specific models of the PF have been considered. In particular, in [44], about a thousand of sources of activation have been used with proper activation times to model the PMJ, whereas in [45], the conduction system has been modeled with a simple network representing the bundle of His and the main bundle branches coupled with a thin layer with discrete sites of activation representing the PF and the PMJ. In the recent work [31], the authors considered the presence of generic accessory pathways with a full biophysical detailed model of the ventricles in a rabbit for the study of tachycardia and arrhythmias.

4.2.2. Discussion of the results. The results reported in Figures 7 and 8 and in Table II for subjects 2 and 3 show again an improvement in the accuracy when the patient-specific network is used instead of the generic one. However, in this case, a deterioration of this improvement can be noticed with respect to the previous case. In particular, for subject 2, the mean error decreased by 23.0%, while for subject 3, it decreased by 25.5%.

Such a deterioration in the performance of the patient-specific network with respect to the previous case can be ascribed to the fact that a percentage of the measurement points (the subset $\mathcal{W}$) is directly activated by the anomalous pathway, and therefore, it is not affected by the presence of the Purkinje network. For subject 2, the one with the worst improvement in accuracy, the subset $\mathcal{W}$ contains 48.0% of the measures in the testing set, while for subject 3, it contains 30.0% of these measures. Therefore, to study the effective improvement in the accuracy obtained by using the patient-specific network, we computed in Table III and Figure 8 the mean error associated only to the measurement points in the subset $\mathcal{K}$, which is those activated, in our simulation, by the PF. These results show that when focusing on the points of $\mathcal{K}$, a better improvement in the accuracy obtained by the patient-specific network is noticed. In particular, for subject 2, the mean error decreased by 33.8%, while for subject 3, it decreased by 34.9%, highlighting the importance of including a patient-specific network at least for the points activated by the network itself. Accordingly, no appreciable improvement is noticed for the measurement points in $\mathcal{W}$, that is, those activated in our simulations by the anomalous pathway.

These results highlighted that for the WPW syndrome, it is important to use a patient-specific Purkinje network when we want to accurately describe the activation in a region of the endocardium far from the anomalous pathway. On the contrary, if we were interested only on the activation near the intramyocardial pathway, a non-patient-specific network could be enough.

5. CONCLUSIONS AND LIMITATIONS

In this work, we proposed a computational algorithm for the generation of a patient-specific Purkinje network in the general case of pathological electrical propagations in the ventricle. In particular, this method can be applied to cases when also muscular sources, in addition to the AV node, contribute to the activation. We applied this method to three cases characterized by electrical pathological propagations. We compared the results obtained by using the patient-specific Purkinje network with the ones given by considering a no patient-specific (generic) network. The numerical results highlighted the following:

1. the improvement in the accuracy obtained by using the patient-specific network in the case of an old myocardial infarction;
2. the importance of considering a patient-specific Purkinje network to detect the specificity of the electrical propagation of the patient at hand, as highlighted in the case of a muscular conduction problem (myocardial ischemia);
3. the reliability of the patient-specific Purkinje network to accurately describe the propagation in the case of the WPW syndrome, in particular far from the anomalous muscular pathway.

These conclusions show that our method provides an effective tool to accurately model the activation of the left ventricle in the case of pathological electrical propagations with different origins, from conduction problems in the myocardium to the presence of an additional muscular pathway.

The main limitation of this work consists in neglecting the re-entry phenomena in the Purkinje network. In particular, we assumed that a signal that starts from the AV node and enters the muscle through a PMJ cannot re-enter the network. We observe that owing to the high values of the orthodromic and antidromic delays at the PMJ, it is reasonable to assume that, at least for not damaged Purkinje networks, the phenomenon of the re-entry does not significantly influence the propagation. A second limitation is given by the use of the eikonal problem to compute the activation times in the left ventricle. Other models, such as the bidomain or the monodomain ones, could be used to provide more accurate results, accounting also for the modeling of the transmembrane potential. Finally, we notice that the aim of this work does not consist in reproducing the *real* Purkinje network. Rather, we wanted to provide an algorithm to generate a *realistic* network able to describe accurately the electrical activation of the patient at hand, capturing its peculiarities.

As next steps of our work, we want to consider also other pathologies, such as the left bundle branch block, with the aim of studying the electrical propagation during the *cardiac resynchronization therapy*. In this case, it will be mandatory to consider also the activation coming from the right ventricle. Moreover, we want to extend our method to consider also the re-entry phenomena and to include more sophisticated models such as the bidomain or the monodomain ones.

ACKNOWLEDGEMENT

The present study has been funded by Fondazione Cassa di Risparmio di Trento e Rovereto (CARITRO) within the project 'Numerical modelling of the electrical activity of the heart for the study of the ventricular dyssynchrony'.

ETHICAL APPROVAL

This clinical study has been approved by the ethic committee of Azienda Provinciale per i Servizi Sanitari, Trento (Italy). The patients have been previously informed and gave their full consent for both the acquisition of the clinical data and the successive mathematical analyses.

REFERENCES

1. Durrer D, van Dam R, Freud G, Janse M, Meijler F, Arzbaecher R. Total excitation of the isolated human heart. *Circulation* 1970; **41**(6):899–912.

2. Rawling DA, Joyner RW, Overholt ED. Variations in the functional electrical coupling between the subendocardial Purkinje and ventricular layers of the canine left ventricle. *Circulation Research* 1985; **57**(2):252–261.
3. Anderson R, Yanni J, Boyett M, Chandler N, Dobrzynski H. The anatomy of the cardiac conduction system. *Clinical Anatomy* 2009; **22**(1):99–113.
4. Relan J, Chinchapatnam P, Sermesant M, Rhode K, Ginks M, Delingette H, Rinaldi CA, Razavi R, Ayache N. Coupled personalization of cardiac electrophysiology models for prediction of ischaemic ventricular tachycardia. *Interface Focus* 2011. DOI: 10.1098/rsfs.2010.0041.
5. Wang D, Kirby R, MacLeod R, Johnson C. Inverse electrocardiographic source localization of ischemia: an optimization framework and finite element solution. *Journal of Computational Physics* 2013; **250**:403–424.
6. Romero D, Sebastian R, Bijnens BH, Zimmerman V, Boyle PM, Vigmond EJ, Frangi AF. Effects of the Purkinje system and cardiac geometry on biventricular pacing: a model study. *Annals of Biomedical Engineering* 2010; **38**(4):1388–1398.
7. Sermesant M, Chabiniok R, Chinchapatnam P, Mansi T, Billet F, Moireau P, Peyrat J, Wong K, Relan J, Rhode K, Ginks M, Lambiase P, Delingette H, Sorine M, Rinaldi C, Chapelle D, Razavi R, Ayache N. Patient-specific electromechanical models of the heart for the prediction of pacing acute effects in CRT: a preliminary clinical validation. *Medical Image Analysis* 2012; **16**(1):201–215.
8. Keller DU, Weiss DL, Dossel O, Seemann G. Influence of heterogeneities on the genesis of the t-wave: a computational evaluation. *IEEE Transactions on Biomedical Engineering* 2012; **59**(2):311–322.
9. Abboud S, Berenfeld O, Sadeh D. Simulation of high-resolution qrs complex using a ventricular model with a fractal conduction system. Effects of ischemia on high-frequency qrs potentials. *Circulation Research* 1991; **68**(6): 1751–1760.
10. Berenfeld O, Jalife J. Purkinje-muscle reentry as a mechanism of polymorphic ventricular arrhythmias in a 3-dimensional model of the ventricles. *Circulation Research* 1998; **2**(10):1063–1077.
11. Ijiri T, Ashihara T, Yamaguchi T, Takayama K, Igarashi T, Shimada T, Namba T, Haraguchi R, Nakazawa K. A procedural method for modeling the Purkinje fibers of the heart. *Progress in Biophysics & Molecular Biology* 2008; **58**(7):90–100.
12. Sebastian R, Zimmerman V, Romero D, Sanchez-Quintana D, Frangi AF. Characterization and modeling of the peripheral cardiac conduction system. *IEEE Transactions on Medical Imaging* 2013; **32**(1):45–55.
13. Tusscher KH, Panfilov AV. Modelling of the ventricular conduction system. *Progress in Biophysics & Molecular Biology* 2008; **96**(1–3):152–170.
14. Palamara S, Vergara C, Faggiano E, Nobile F. An effective algorithm for the generation of patient-specific Purkinje networks in computational electrocardiology. *MOX-Report n. 48-2013*, Dipartimento di Matematica, Politecnico di Milano: Italy, 2013.
15. Vergara C, Palamara S, Catanzariti D, Pangrazzi C, Nobile F, Centonze M, Faggiano E, Maines M, Quarteroni A, Vergara G. Patient-specific generation of the Purkinje network driven by clinical measurements of a normal propagation. *Medical & Biological Engineering & Computing* 2014; **52**(10):813–826.
16. Yushkevich P, Piven J, Hazlett HC, Smith RG, Ho S, Gee JC, Gerig G. User-guided 3D active contour segmentation of anatomical structures: significantly improved efficiency and reliability. *Neuroimage* 2006; **31**(3):1116–1128.
17. Rotter M, Takahashi Y, Sanders P, Haïssaguerre M, Jaïs P, Hsu L, Sacher F, Pasquié J, Clementy J, Hocini M. Reduction of fluoroscopy exposure and procedure duration during ablation of atrial fibrillation using a novel anatomical navigation system. *European Heart Journal* 2005; **26**(14):1415–1421.
18. Wittkampf FHM, Wever EFD, Derksen R, Wilde AAM, Ramanna H, Hauer RNW, De Medina EOR. LocaLisa new technique for real-time 3-dimensional localization of regular intracardiac electrodes. *Circulation* 1999; **99**(10): 1312–1317.
19. Bhakta D, Miller JM. Principles of electroanatomic mapping. *Indian Pacing and Electrophysiology Journal* 2008; **8**(1):32-50.
20. Eitel C, Hindricks G, Dagres N, Sommer P, Piorkowski C. Ensite velocity cardiac mapping system: a new platform for 3D mapping of cardiac arrhythmias. *Expert Review of Medical Devices* 2010; **7**(2):185–192.
21. Clayton RH, Bernus O, Cherry EM, Dierckx H, Fenton FH, Mirabella L, Panfilov AV, Sachse FB, Seemann G, Zhang H. Models of cardiac tissue electrophysiology: Progress, challenges and open questions. *Progress in Biophysics and Molecular Biology* 2011; **104**(1–3):22–48.
22. Colli Franzone P, Pavarino L. A parallel solver for reaction diffusion systems in computational electrocardiology. *Mathematical Methods in the Applied Sciences* 2004; **14**(06):883–911.
23. Keener J, Bogar K. A numerical method for the solution of the bidomain equations in cardiac tissue. *Chaos* 1998; **8**(1):234–241.
24. Vigmond E, Aguel F, Trayanova N. Computational techniques for solving the bidomain equations in three dimensions. *IEEE Transactions on Biomedical Engineering* 2002; **49**(11):1260–1269.
25. Colli Franzone P, Guerri L. Spreading excitation in 3-d models of the anisotropic cardiac tissue, I. validation of the eikonal model. *Mathematical Biosciences* 1993; **113**:145–209.
26. Keener J. An eikonal-curvature equation for action potential propagation in myocardium. *Journal of Mathematical Biology* 1991; **29**(7):629–651.
27. Tobon-Gomez C, Duchateau N, Sebastian R, Marchesseau S, Camara O, Donal E, Craene MD, Pashaei A, Relan J, Steghofer M, Lamata P, Delingette H, Duckett S, Garreau M, Hernandez A, Rhode K, Sermesant M, Ayache N, Leclercq C, Razavi R, Smith N, Frangi A. Understanding the mechanisms amenable to CRT response: from

pre-operative multimodal image data to patient-specific computational models. *Medical & Biological Engineering & Computing* 2013; **51**(11):1235-1250. DOI: 10.1007/s11517-013-1044-7.
28. Rossi S, Lassila T, Ruiz-Baier R, Sequeira A, Quarteroni A. Thermodynamically consistent orthotropic activation model capturing ventricular systolic wall thickening in cardiac electromechanics. *European Journal of Mechanics-A/Solids* 2014; **48**:129-142. DOI: 10.1016/j.euromechsol.2013.10.009.
29. Kerckoffs B, Faris O, Boveenderd P, Prinzen F, Smits K, Arts T. Timing of depolarization and contraction in the paced canine left ventricle. *Journal of Cardiovascular Electrophysiology* 2003; **14**:S188–S195.
30. Huelsing DJ, Spitzer KW, Cordeiro JM, Pollard AE. Conduction between isolated rabbit Purkinje and ventricular myocytes coupled by a variable resistance. *American Journal of Physiology-Heart and Circulatory Physiology* 1998; **274**(4):H1163–H1173.
31. Boyle P, Veenhuyzen G, Vigmond E. Fusion during entrainment of orthodromic reciprocating tachycardia is enhanced for basal pacing sites but diminished when pacing near Purkinje system end points. *Heart Rhythm* 2013; **10**(3):444–451.
32. Sebastian R, Zimmerman V, Romero D, Frangi A. Construction of a computational anatomical model of the peripheral cardiac conduction system. *Progress in Biophysics & Molecular Biology* 2011; **58**(12):90–100.
33. Bogun F, Good E, Reich S, Elmouchi D, Igic P, Tschopp D, Dey S, Wimmer A, Jongnarangsin K, Oral H, *et al.* Role of Purkinje fibers in post-infarction ventricular tachycardia. *Journal of the American College of Cardiology* 2006; **48**(12):2500–2507.
34. Lombaert H, Peyrat J, Croisille P, Rapacchi S, Fanton L, Cheriet F, Clarysse P, Magnin I, Delingette H, Ayache N. Human atlas of the cardiac fiber architecture: study on a healthy population. *IEEE Transactions on Medical Imaging* 2012; **31**(7):1436–1447.
35. Iaizzo PA. *Handbook of Cardiac Anatomy, Physiology, and Devices*. Springer: New York City, 2009.
36. Frazier DW, Krassowska W, Chen PS, Wolf PD, Danieley ND, Smith WM, Ideker RE. Transmural activations and stimulus potentials in three-dimensional anisotropic canine myocardium. *Circulation Research* 1988; **63**(1):135–146.
37. Dubé B, Gulrajani RM, Lorange M, LeBlanc A, Nasmith J, Nadeau RA, *et al.* A computer heart model incorporating anisotropic propagation: IV. Simulation of regional myocardial ischemia. *Journal of Electrocardiology* 1996; **29**(2):91–103.
38. Hopenfeld B, Stinstra JG, MacLeod RS. The effect of conductivity on st-segment epicardial potentials arising from subendocardial ischemia. *Annals of Biomedical Engineering* 2005; **33**(6):751–763.
39. Stinstra JG, Shome S, Hopenfeld B, MacLeod RS. Modelling passive cardiac conductivity during ischaemia. *Medical and Biological Engineering and Computing* 2005; **43**(6):776–782.
40. Nielsen BF, Lysaker M, Grottum P. Computing ischemic regions in the heart with the bidomain model first steps towards validation. *IEEE Transactions on Medical Imaging* 2013; **32**(6):1085–1096.
41. Nogami A. Purkinje-related arrhythmias part II: polymorphic ventricular tachycardia and ventricular fibrillation. *Pacing and Clinical Electrophysiology* 2011; **34**(8):1034–1049.
42. van Dam PM, Oostendorp TF, van Oosterom A. Application of the fastest route algorithm in the interactive simulation of the effect of local ischemia on the ECG. *Medical & Biological Engineering & Computing* 2009; **47**(1):11–20.
43. Tai C-T, Chen S-A, Chiang C-E, Wu T-J, Cheng C-C, Chiou C-W, Lee S-H, Ueng K-C, Chang M-S. Accessory atrioventricular pathways with only antegrade conduction in patients with symptomatic Wolff–Parkinson–White syndrome clinical features, electrophysiological characteristics and response to radiofrequency catheter ablation. *European Heart Journal* 1997; **18**(1):132–139.
44. Lorange M, Gulrajani RM. Computer simulation of the Wolff–Parkinson–White preexcitation syndrome with a modified Miller–Geselowitz heart model. *IEEE Transactions on Biomedical Engineering* 1986; **BME-33**(9):862–873.
45. Killmann R, Wach P, Dienstl F. Three-dimensional computer model of the entire human heart for simulation of reentry and tachycardia: gap phenomenon and Wolff–Parkinson–White syndrome. *Basic Research in Cardiology* 1991; **86**(5):485–501.